Zhang *et al. Journal of Ovarian Research* (2025) 18:95
https://doi.org/10.1186/s13048-025-01672-9

Journal of Ovarian Research

RESEARCH Open Access

Restoration of TP53 strategy via specific nanoparticles for ovarian cancer therapy

Menglei Zhang[1,2†], Yuanyuan Gu[1,2†], Fang Shen[1,2†], Yingxin Gong[1], Zheng Gu[1], Keqin Hua[1*†], Guannan Zhou[1,2*†] and Jingxin Ding[1*†]

Abstract

The p53 tumor suppressor gene, a master regulator of diverse cellular pathways, is frequently altered in various cancers. Loss of function in tumor suppressor genes is commonly associated with the onset/progression of cancer and treatment resistance. Currently, approaches for restoration of TP53 expression, including small molecules and DNA therapies, have yielded progressive success, but each has formidable drawbacks. Here, we introduced an endogenous nanoplatform to effectively deliver the TP53 protein. Briefly speaking, the endogenous TP53 proteins were fused by the Lamp2b and loaded into extracellular vesicles-based nanoparticles, which could markedly restore the TP53 expression in natural TP53-deficient ovarian cancer (OCs) and subsequently inhibit cell proliferation as well as induce cell apoptosis. Moreover, a well-known biotin streptavidin binding strategy was used to confer the nanoplatform targeting ability. Since mesothelin (MSLN) expressed highly in ovarian cancer, the anti-MSLN nanoplatform were engineered to deliver TP53 proteins to MSLN ovarian cancer and exert the anti-tumor ability. Our findings indicated that restoration of tumor suppressors by the targeting nanoplatform could be promising nanotechnology approaches for potential ovarian cancer treatment.

Keywords Nanoplatform, TP53, Ovarian cancer, Targeting, Engineering

Introduction

It is widely acknowledged that TP53 is a transcription factor that triggers growth inhibitory and apoptotic responses to a wide range of insults, including DNA damage, stress, and oncogene activation [1]. Induction of cell-cycle arrest, apoptosis, and senescence are among the earliest discovered functions of TP53, effectively counteracting the rapid proliferation of cancer cells and contributing to tumor suppression. However, the TP53 is lost or mutated in approximately half of human cancers, which results in promote tumor proliferation, invasion, and drug resistance [2]. Owing to the vital role of TP53 function during tumorigenesis in suppressing the emergence of incipient tumors, TP53 was widely acknowledged as "Guardian of the genome" [3]. The TP53 is frequently altered in various cancers, which was observed to occur in approximately more than 30%

†Menglei Zhang, Yuanyuan Gu and Fang Shen contributed equally to this work.

†Keqin Hua, Guannan Zhou and Jingxin Ding contributed equally to this work.

*Correspondence:
Keqin Hua
huakeqinjiaoshou@163.com
Guannan Zhou
zgnsmmu@163.com
Jingxin Ding
djxdd@sina.com

Full list of author information is available at the end of the article

Graphical Abstract

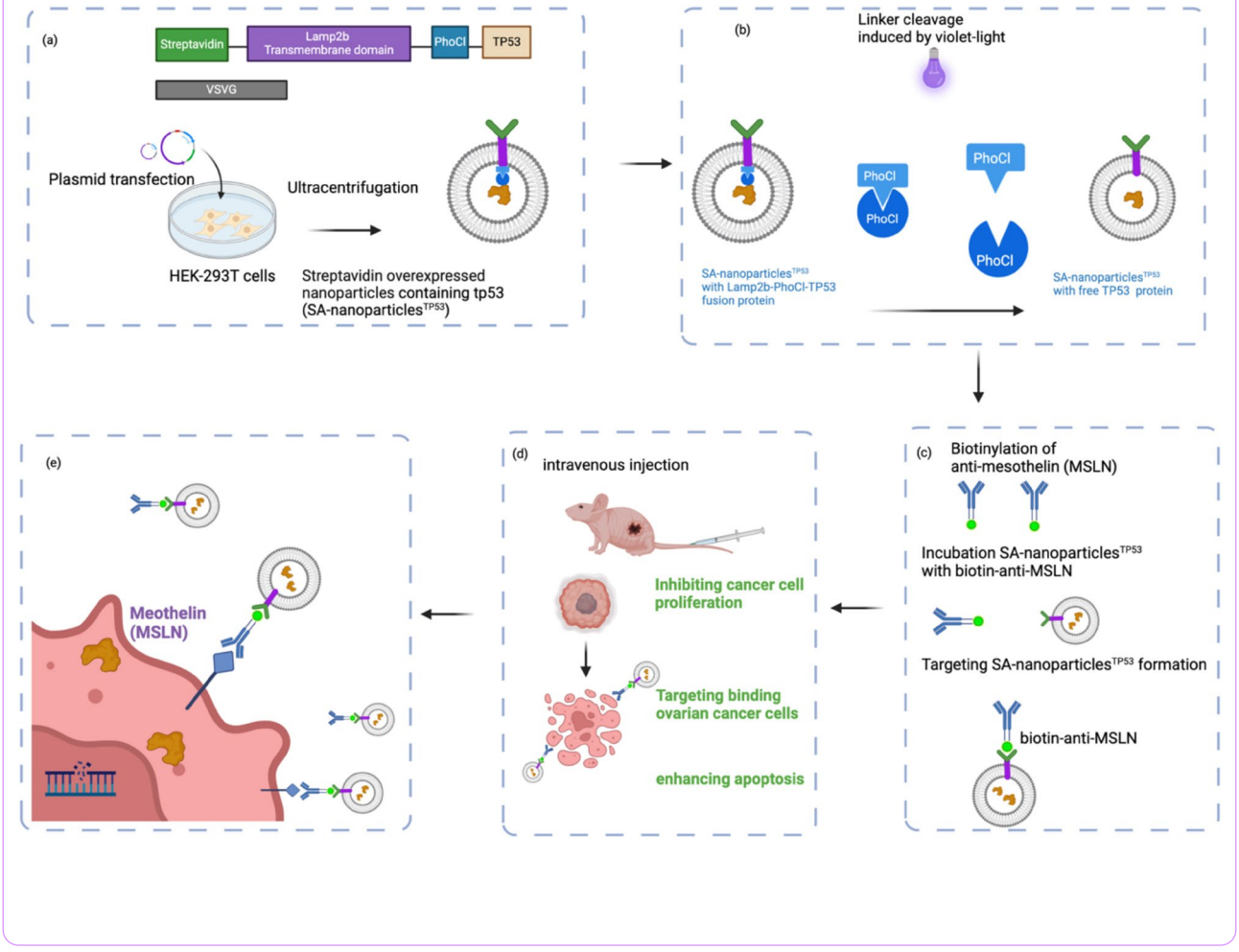

of hepatocellular carcinomas (HCCs) cases and in more than 40% of ovarian cancer (OCs) [4] cases, as well as in more than 90% high-grade serous OC cases [5]. Recently, increasing studies has developed multiple strategies for targeting dysfunctional TP53 in cancer treatment [6–8]. Thus, the restoration of TP53 function is becoming an attractive and promising tumor-specific therapeutic strategy. The tumor suppressor gene TP53 produces a protein that is essential for halting the development of cancer. It helps monitoring of the genome's integrity. When DNA damage occurs, TP53 can cause apoptosis or cell cycle arrest, depending on whether the damage can be repaired or is irreversible [9, 10]. Targeting of tumor-suppressing TP53 by the synthetic mRNA NP delivery could lead to remarkable antitumor effects in vitro and in multiple animal models of HCC and NSCLC [6]. Recently, studies reported that the anti-aggregation peptide ReACp53 could rescues TP53 function in cancer cell lines and in organoids derived from high-grade serous ovarian carcinomas (HGSOC) [11, 12] and could significantly decrease the p53 mutants mediated gain of oncogenic functions (GOFs) and chemoresistance [13, 14]. These findings highlight a role of ERP29 in the acquired chemoresistance of cancer cells expressing the aggregating TP53 mutant Arg282Trp. Our results also suggest that ERP29-mediated GOF can be targeted by the anti-aggregation peptide ReACp53. Thus, the TP53 restoration strategy is a promising therapy in treating cancer, particular in TP53 deficient malignancies [6].

Increasing nanoplatforms were reported to applied to achieve the drug delivery including Lipid Nanoparticles (LNP) [15], Adeno-associated viruses (AAV) [16], cell penetrating peptides (CPPs) [17], extracellular vesicles (EVs) [18], engineered bacteria [19] and so on. However, LNPs are currently widely used platform for delivery. However, their limited capacity to undergo endosomal escape limits the use of LNPs as RNA delivery vehicles [20]. AAV vectors are promising in gene therapy for their stable, efficient, and non-cytotoxic gene delivery to transduce a great number of tissues of different mammalian

species. However, AAV-based therapy also has some problems, including pre-existing AAV-neutralizing antibodies in the body and inability to target specific cells [21]. The possible interactions between CPPs and other proteins, as well as the potential cytotoxicity limit the application of CPPs [22]. Nanovesicles sizes range from 30 nm to150 nm in diameter (including EVs [23], sEVs [24], exomeres [25] and so on) secreted by diverse cells through the paracrine pathway [26] have been widely acknowledged as vital nanocarriers for transferring signaling as well as cargoes. With the increasing studies upon EVs biogenesis process, EVs-based nanoparticles system have been reported as promising nanocarrier candidates for loading as well as transmitting biological cargoes (including mRNA [27, 28], miRNAs [29, 30] and proteins [31]) between diverse cells and tissues [31, 32] to mediate the biological processes of tumor immunity as well as the inflammatory response [33–36]. In recent years, EVs-based delivery system plays roles in delivering cargoes (including the genome editing tools [37], mRNAs [38, 39], siRNAs [40–42] and proteins) via their excellent loading ability [43, 44]. Meanwhile, photocleavable protein is one of recently reported protein linkers for the drug delivery field [45]. Based on the photocleavable proteins, it is available to load the protein of interest into the nanoparticles for further delivery and release, which means cargo proteins can be loaded into the nanoparticles by fusing them with photocleavable protein-conjugated membrane markers (Lamp2b [46], CD63 [47], CD81 [48] and so on) and subsequently released from the nanoparticles membrane by inducing photocleavage with blue light illumination [49]. Herein, in this present study, we produced bioengineered nanoparticles to load the TP53 proteins to form nanoparticles^{TP53} and subsequently be delivered into the receipt cells (both artificial TP53 deficient cells and the natural TP53-low cancer cells) to inhibit the above cancer cells. Considering MSLN is emerging as an attractive target for ovarian cancer immunotherapy due to its low expression on normal mesothelial cells and high expression in ovarian cancers. We formed the anti-MSLN nanoparticles^{TP53} to target the ovarian cancer cells. The specific anti-MSLN nanoplatforms^{TP53} could targeting the ovarian cancer and significantly inhibit the suppress the SKOV-3 tumor growth in vivo. Above all, the specific targeting bioengineered EVs could load and deliver TP53 specifically to inhibit ovarian cancer in vitro and in vivo. This study could provide theoretical basis of the potential application for bioengineered nanoplatforms to deliver bioactive proteins in cancer treatment.

Results

The expression level of TP53 in ovarian cancer

To clarify the vital role of TP53 in the progression of ovarian cancer, we selected the SKOV-3 cells as the TP53-low cancer cells. As depicted in Fig. 1, the result derived from Cancer Cell Line Encyclopedia (CCLE) DataSet [50, 51] showed that SKOV-3 cancer cells express lowest level of TP53 not only among the whole cancer cells in primary sites (Fig. 1A), but also among the metastasis sites (Fig. 1B). Furthermore, as demonstrated in NCI-60 cell lines DataSet, the mutant type of SKOV-3 cancer cells is Deletion – Frameshift (Supplementary Table S1). These results are consistence with the results from previous studies [6, 52, 53] that ovarian cancer is TP53 deficient cancer. Above all, SKOV-3 cancer cell is a cancer cell line with deficient TP53 expression, which is a promising candidate for TP53 delivery evaluation.

Loading strategy of endogenous proteins into bioengineered nanoparticles

We designed a nanoplatform based on small EVs-based nanoparticles for delivery, which could fuse the proteins of interests into the nanoparticles during the biogenesis process. Firstly, we designed the plasmid to transfect the original cells for nanoparticles producing. As depicted in Fig. 2A, the plasmid contains (i) the transmembrane part "Lamp2b", (ii) photocleavable protein domain "PhoCl" for releasing free protein and (iii) cargo protein "cargo". Since the "Lamp2b" could express stable via transmembrane in nanoplatforms, the "PhoCl-protein of interest" could be linked expressed and sorted into the nanoplatforms (Fig. 2B). After the 405 nm violet light treatment, the 405 nm light-cleavable linker could be cleaved, and the protein of interest could be released freely into the nanoparticles (Fig. 2C). Based on this strategy, the plasmid could translate the fused protein during the nanoparticles biogenesis in the origin cells (CHO cells) and subsequently load the proteins of interest into the nanoparticles (Fig. 2).

Isolation and characterizations of bioengineered nanoparticles

After the transfection, the supernatant from origin CHO cells was collected for nanoparticles isolation. And after the ultra-centrifugation and purification, the EVs were collected for further evaluation. Briefly, we conducted the transmission electron microscopy (TEM) to evaluate the shape of the EVs and conducted the Nanoparticle tracking analysis (NTA) to evaluate the size distribution of the nanoparticles. In addition, we conducted the western blot to evaluate the markers of nanoparticles. As depicted in Fig. 2D, both the nanoparticles encapsulated TP53 (nanoparticles^{TP53}) and blank nanoparticles exhibited classic cup-shaped structure. In addition, as

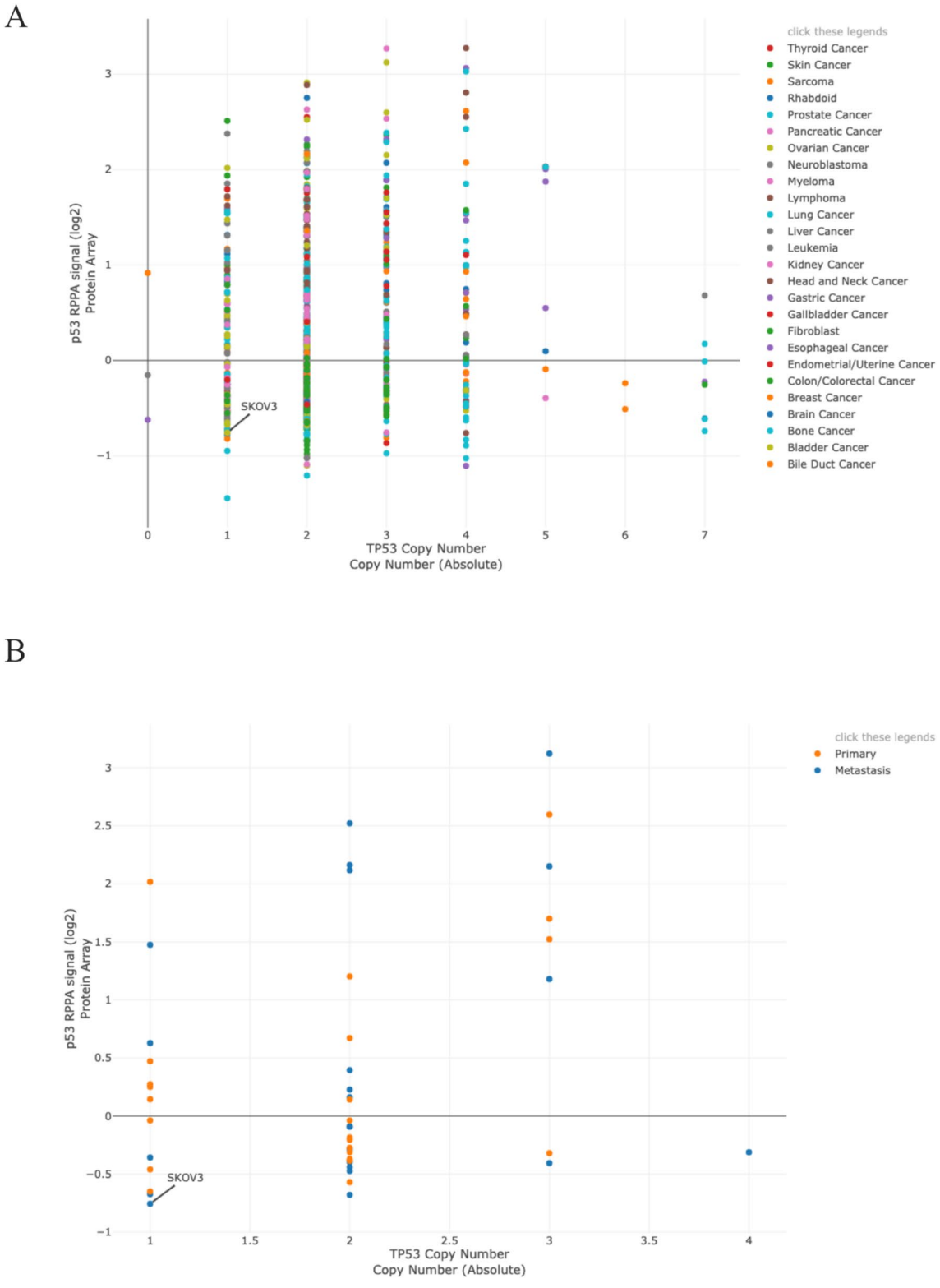

Fig. 1 Procedure of biogenesis of bioengineered nanoparticles^{TP53} and Characterization of nanoparticles^{TP53}. (**A**) Schematic illustrating the TP53 aberrant cancer cells by site. X axis: TP53 copy number (absolute), Y axis: P53 RPPA signal (log_2) protein array. (**B**) Schematic illustrating the TP53 expression in primary site and metastatic site of cancer cells. X axis: TP53 copy number (absolute), Y axis: P53 RPPA (log_2) signal protein array

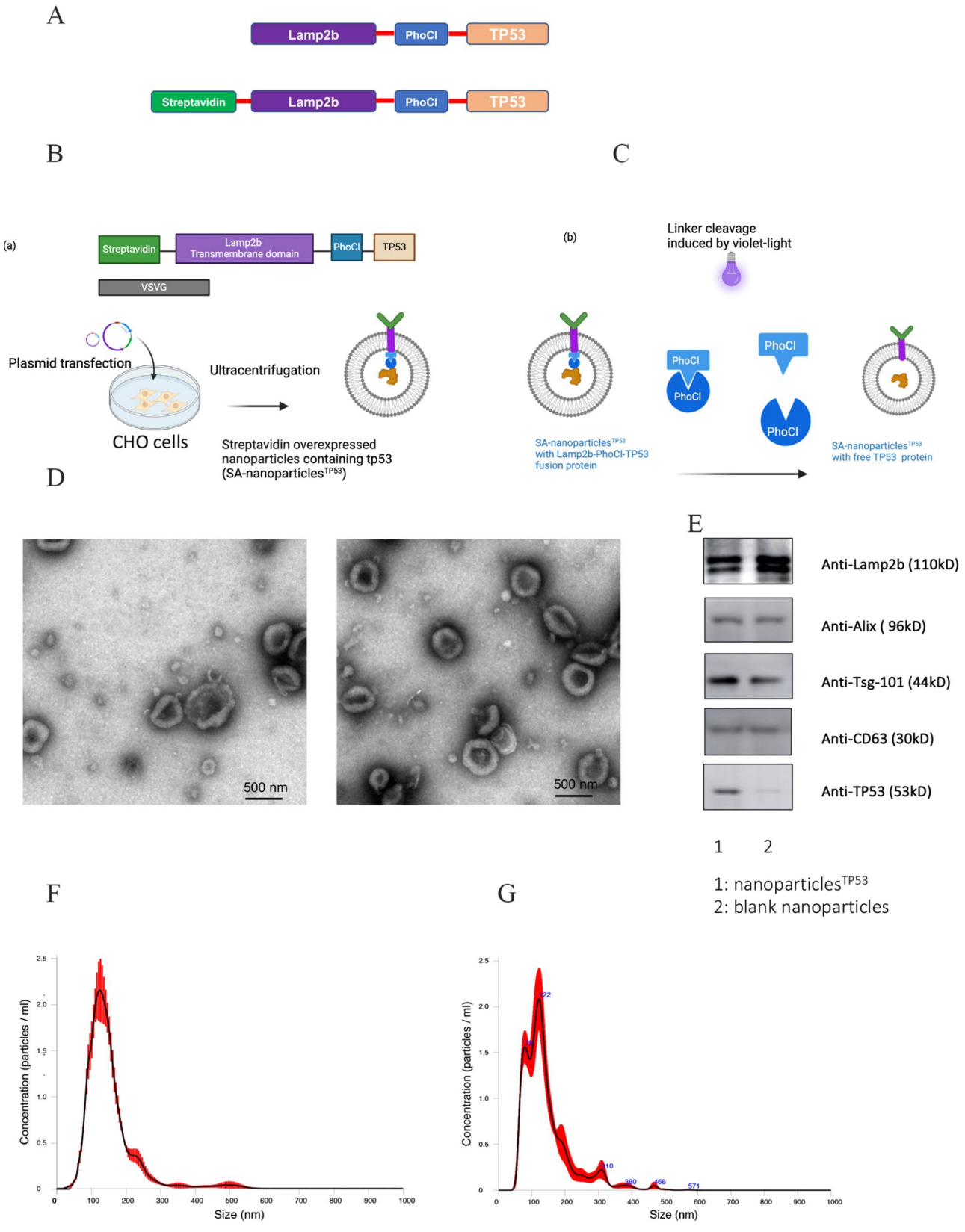

Fig. 2 (See legend on next page.)

(See figure on previous page.)

Fig. 2 Procedure of biogenesis of bioengineered nanoparticles^{TP53} and Characterization of nanoparticles^{TP53}. **A**. Schematic illustrating the plasmids to produce the nanoparticles^{TP53} and SA-nanoparticles^{TP53}. **B**. Schematic illustrating the biogenesis process of nanoparticles^{TP53} and SA-nanoparticles^{TP53}. **C**. Schematic illustrating the PhoCl protein be cleaved after 405 nm violet light treatment to release the cargoes of interests. **D**. TEM images of purified nanoparticles^{TP53}(left) and blank nanoparticles (right). Scale bar, 500 nm. **E**. Biomarkers, sorting protein and cargoes of interests, negative marker in nanoparticles were detected by western blotting. **F**. NTA analysis of purified nanoparticles^{TP53}. **G**. NTA analysis of purified blank nanoparticles

the results from western blot, both nanoparticles^{TP53} and blank nanoparticles exhibited the expression of EVs-specific markers CD63, Alix, Tsg101 and absent of the expression of GRP94 (previous reported EVs negative marker [54]). Both the nanoparticles^{TP53} and the blank nanoparticles could express the sorting protein Lamp2b, while only the nanoparticles^{TP53} containing TP53, suggesting that the TP53 has been successfully loaded into the purified nanoparticles^{TP53} by Lamp2b through the biogenesis process (Fig. 2E and Figure S1). Furthermore, the size of these nanoparticles ranged from 30 nm to 1000 nm (Fig. 2F and G). Collectively, the delivery platform strategy could sort and load the proteins of interest into the bioengineered nanoparticles.

Uptake of nanoparticles containing diverse cargoes in recipient cells

To explore whether the bioengineered nanoparticles could enter the recipient cells, we conducted the nanoparticles uptake assay (Fig. 3). We stained the nanoparticles by PKH26 dye, then used the PKH26-labeled nanoparticles to treat the SKOV-3 cells (Fig. 3A). As demonstrated in Fig. 3B, the PKH-26 labeled nanoparticles could be encapsulated by the FITC-Actin-Tracker labeled SKOV-3 cells. In addition, we produced the bioengineered nanoparticles to load other bioactive proteins: (1) GFP proteins (Fig. 3C) and (2) luciferase proteins (Fig. 3H), then detected the delivery efficiency in recipient cells. It is demonstrated that 10^{10} particles could reach the delivery plateau with not significant cytotoxicity (Figure S3A and 3B). As depicted in Fig. 3D and E, the bioengineered nanoparticles^{GFP} could be encapsulated by the SKOV-3 cells, and result in the treated SKOV-3 cells express green fluorescence, while the blank nanoparticles and PBS could not result in the treated SKOV-3 cells express green fluorescence. Also, the results from the flow cytometry assays concluded the similar results with the immune fluorescence microscopy assay (Fig. 3F and G). Meanwhile, we used the plasmid "Lamp2b-PhoCl-Luciferase" to transfect origin cells for producing nanoparticles^{Luciferase}, which were used to treat the SKOV-3 cells for 24 h (Fig. 3H). As depicted in Fig. 3L, the nanoparticles^{Luciferase} treated SKOV-3 cells could express remarkable luciferase activity, while the blank nanoparticles and PBS could not result in luciferase activity. Furthermore, we used the plasmid "Lamp2b-PhoCl-Cre" to produce nanoparticles^{Cre}, which could load the Cre recombinant protein into the bioengineered nanoparticles^{Cre} (Fig. 3J). It is widely acknowledged that the Cre recombinant protein could edit the "Loxp-mCherry-Loxp-GFP" sequences in the SKOV-3$^{Cre-Loxp}$ cells, which were prepared by the lentivirus to express Cre-Loxp in the SKOV-3 stably cells. Thus, the GFP positive percentage of the treated SKOV-3$^{Cre-Loxp}$ cells could reflect the functional delivery ability of the bioengineered nanoparticles. As demonstrated in Fig. 3I, the nanoparticles^{Cre} could edit the SKOV-3$^{Cre-Loxp}$ cells and turn the SKOV-3$^{Cre-Loxp}$ cells from red fluorescence to green fluorescence (Fig. 3I, K and M) while the blank nanoparticles and PBS could not result in fluorescence transformation, which means the bioengineered nanoparticles^{Cre} could delivery Cre recombinant protein functionally. Collectively, the bioengineered nanoparticles could load the protein of interest into the nanoparticles and functional deliver the protein of interest into the recipient cells.

Specific targeting strategy could enhance the delivery efficiency of nanoparticles in vitro

While the unspecific binding impedes the clinical application of delivery system, it is vital to develop the specific targeting strategies for bioengineered nanoparticles. We designed the plasmid "Streptavidin-Lamp2b-PhoCl-Cre" contains four parts as below: (1) the specific targeting domain "Streptavidin", which could bind biotinylated antibodies (such as biotin-Anti Her2+), (2) the transmembrane domain "Lamp2b", which could both sort the cargoes and finish the surface display, (3) photocleavable protein domain "PhoCl" for releasing free protein and (4) cargo protein "Cre". These four parts could produce the nanoparticles containing "Streptavidin-Lamp2b-PhoCl-Cre", named SA-nanoparticles^{Cre}. Then the SA-nanoparticles^{Cre} were incubated with the biotin-Anti-Her2 to prepare the anti-Her2 nanoparticles^{Cre} (Fig. 4A). We added the anti-Her2 nanoparticles^{Cre} into the Her2 + SKOV-3$^{Cre-Loxp}$ cells to detect the percentage of GFP positive of Her2 + SKOV-3$^{Cre-Loxp}$ cells, which could indicate the effectiveness of specific targeting. As demonstrated in Fig. 4B, both the anti-Her2 nanoparticles^{Cre} and nanoparticles^{Cre} could edit the Her2 + SKOV-3$^{Cre-Loxp}$ cells, the GFP positive percentage of treated with anti-Her2 nanoparticles^{Cre} is remarkable higher than the non-targeting nanoparticles^{Cre} treatment (Fig. 4C and D). Collectively, the specific targeting strategy of bioengineered nanoparticles could deliver the cargoes functionally into the targeted recipient cells with high efficiency.

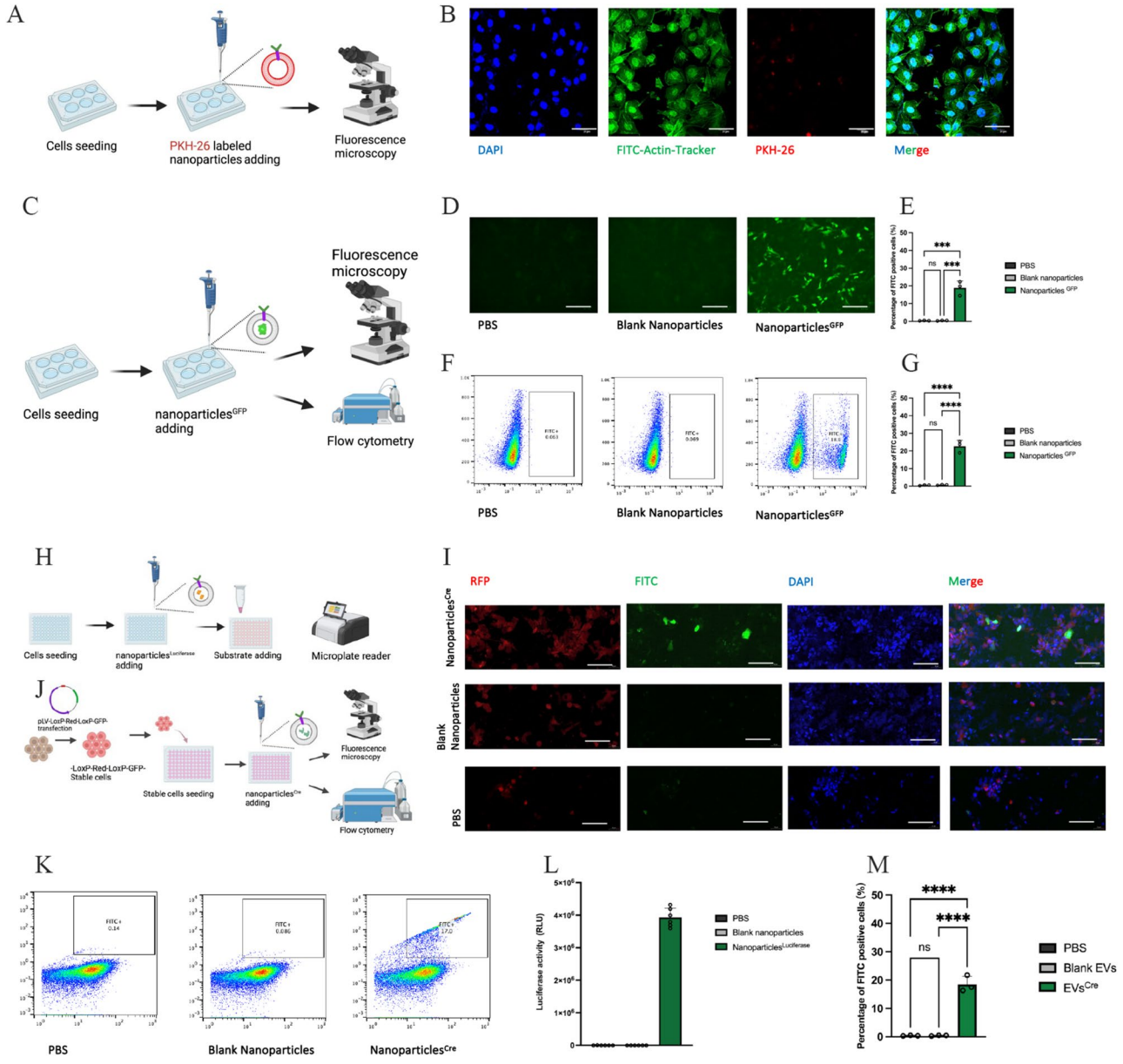

Fig. 3 Uptake of nanoparticles encapsulated diverse cargoes in recipient cells. **A**. Schematic illustrating the flowchart to evaluate the uptake of PKH-26 labeled nanoparticles^{TP53}. **B**. the image (left) and magnify image of PKH-26 (red) labeled nanoparticles entered FITC-actin tracker (green) labeled SKOV-3 cells. Scale bar, 50 μm. **C**. Schematic illustrating the flowchart to evaluate the uptake of nanoparticles^{GFP}. **D**. The fluorescent microscopy was conducted upon the SKOV-3 cells after treated by PBS, blank nanoparticles, nanoparticles^{GFP}. The experiment was repeated three times. Scale bar, 50μm. **E**. The quantitative image of the GFP positive SKOV-3 cells after nanoparticles^{GFP} treatment for Fig. 3D. $p < 0.05$, $n = 3$. **F**. The flow cytometry results of the SKOV-3 cells after treated by PBS, blank nanoparticles, nanoparticles^{GFP}. The experiment was repeated three times. **G**. The quantitative image of the GFP positive SKOV-3 cells after nanoparticles^{GFP} treatment for Fig. 3F. $p < 0.05$, $n = 3$. **H**. Schematic images of the procedure to detect the uptake of nanoparticles^{Luciferase}. **I**. The fluorescent microscopy was conducted upon the SKOV-3$^{Cre-Loxp}$ cells after treated by PBS, blank nanoparticles, nanoparticles^{Cre}. Scale bar, 50μm. **J**. Schematic illustrating the procedure to detect the editing efficiency of nanoparticles^{Cre} in SKOV-3$^{Cre-Loxp}$ cells. **K**. The flow cytometry results of the editing efficiency of nanoparticles in SKOV-3$^{Cre-Loxp}$ after treated by PBS, blank nanoparticles, nanoparticles^{Cre}. The experiment was repeated three times. **L**. The luciferase activity of cells treated by nanoparticles^{Luciferase}. The experiment was repeated three times. **M**. The quantitative image of the editing efficiency of nanoparticles^{Cre} in SKOV-3$^{Cre-Loxp}$ cells from flow cytometry results. $p < 0.05$, $n = 3$

Nanoparticles could inhibit cell viability in artificial TP53-deficient cancer cells HCC$^{p53-/-}$ and native TP53-low cancer cells SKOV-3 in vitro

Based on the vital role of TP53 protein in the cancer progression, we produced bioengineered anti-Her2 nanoparticles^{TP53}. The anti-Her2 nanoparticles^{TP53}, nanoparticles^{TP53}, blank nanoparticles and PBS were added into the artificial TP53-deficient cancer cell

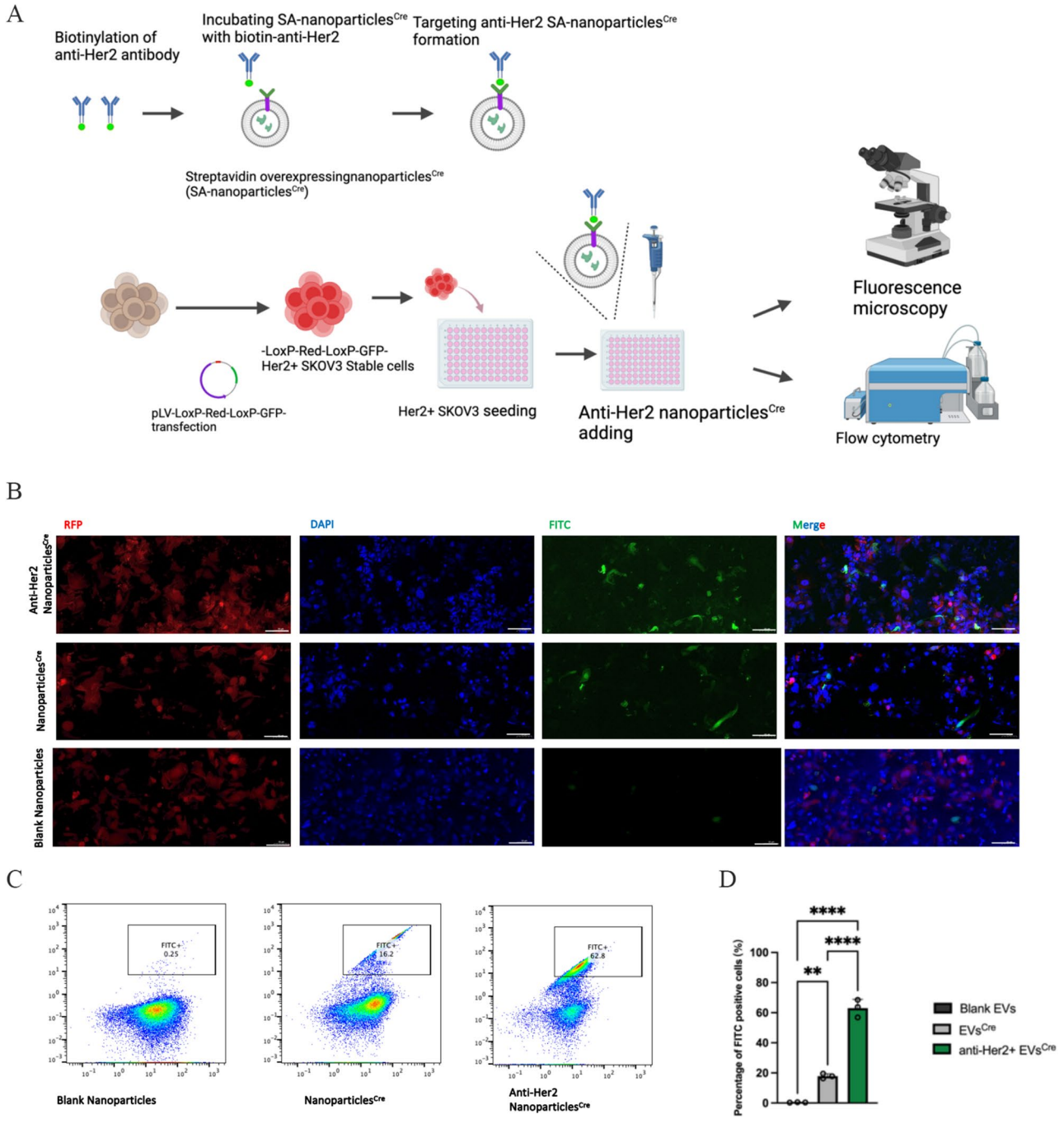

Fig. 4 Specific targeting strategy could enhance the delivery efficiency of nanoparticles in vitro. **A**. Schematic images of the flowchart to detect the uptake of anti-Her2 nanoparticles^{Cre} into Her + SKOV-3$^{Cre-Loxp}$ cells. **B**. The fluorescent microscopy was conducted upon the Her + SKOV-3$^{Cre-Loxp}$ cells after treated by anti-Her2 nanoparticles^{Cre}. Representative data shown; $n = 3$ independent experiments. Scale bar, 50μm. **C**. The flow cytometry result of the Her + SKOV-3$^{Cre-Loxp}$ cells after treated by anti-Her2 nanoparticles^{Cre}. The experiment was repeated three times. **D**. The quantitative image of the editing efficiency of anti-Her2 nanoparticles^{Cre} in the Her + SKOV-3$^{Cre-Loxp}$ cells. $p < 0.05$, $n = 3$

HCC$^{p53-/-}$ and native TP53-low cancer cells SKOV-3, separately. As the results demonstrated in Fig. 5A for cell proliferation assay, the viability of HCC$^{p53-/-}$ (not express Her2 (Figure S3C)) after the treatment with anti-Her2 nanoparticles^{TP53} and nanoparticles^{TP53} are lower than that treated with blank nanoparticles and PBS. Meanwhile, there is no significant difference between the anti-Her2 nanoparticles^{TP53} treatment and nanoparticles^{TP53} treatment (Fig. 5B). In addition, beyond the artificial TP53-deficient cancer cells, we found the similar result in the native TP53-low cancer cells (SKOV-3). The viability of Her2 + SKOV-3 cells treated with anti-Her2

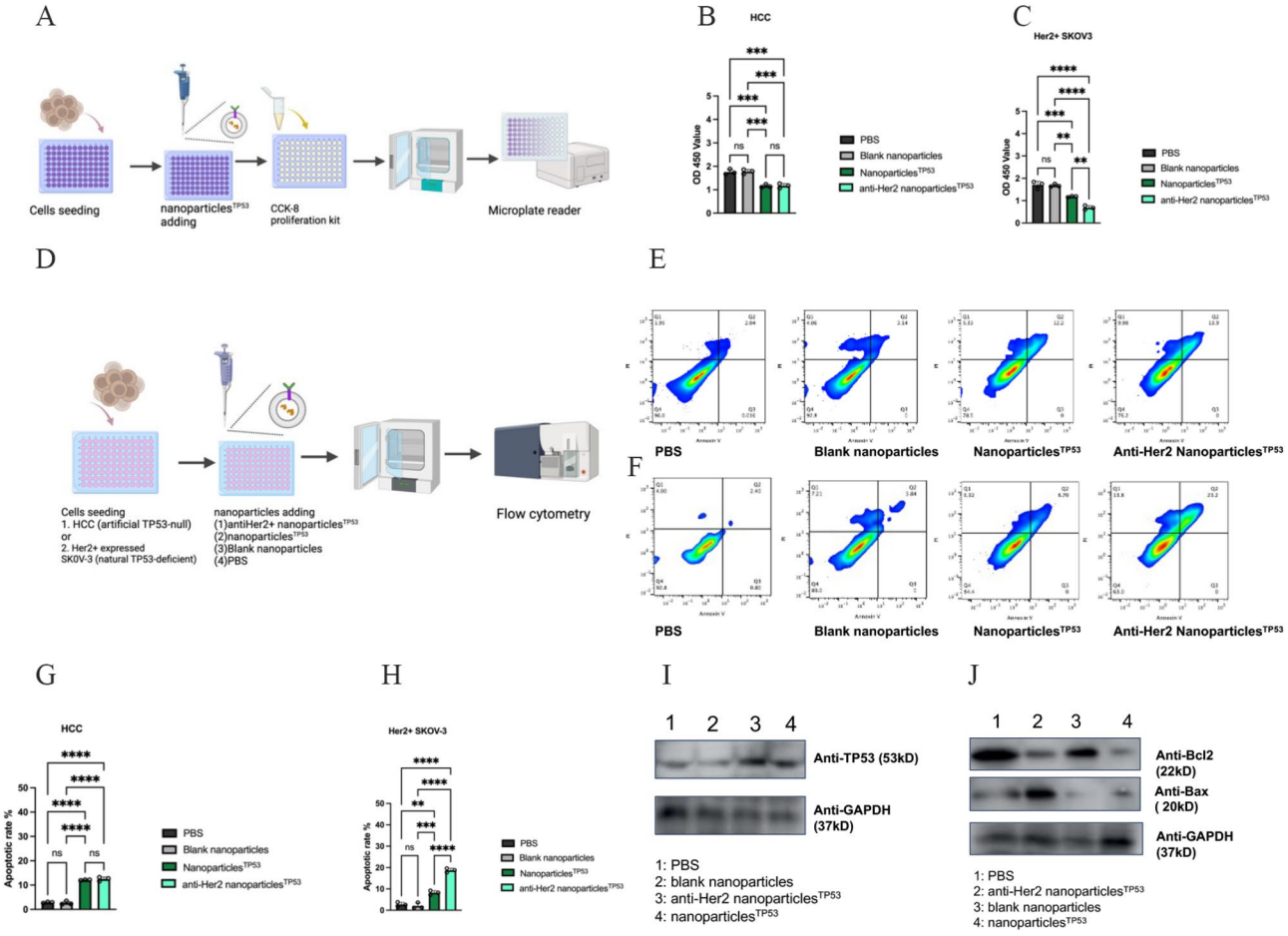

Fig. 5 Nanoparticles^{TP53} could inhibit cell viability in artificial TP53-deficient cancer cells HCC$^{P53-/-}$ and native TP53-low cancer cells SKOV-3 in vitro. **A**. Schematic image of the procedure to detect the effect of nanoparticles^{TP53} on the viability of artificial TP53 deficient HCCs and natural TP53 deficient OCs. **B**. The nanoparticles^{TP53} inhibit the cell viability of HCC cells. Representative data shown; $n=3$ independent experiments. **C**. The Anti-Her2 nanoparticles^{TP53} exhibited greater inhibition of the cell viability than other groups in Her2 + SK-OV-3 cells. Representative data shown; $n=3$ independent experiments. **D**. Schematic illustrating the procedure to detect the effect of Anti-Her2 nanoparticles^{TP53} on the apoptosis of artificial TP53 deficient HCCs and natural TP53 deficient OCs. **E**. The nanoparticles^{TP53} promote the apoptosis of HCC cells. The experiment was repeated three times. **F**. The Anti-Her2 nanoparticles^{TP53} expressed greater inhibition of the cell viability than other groups in Her2 + SK-OV-3 cells. Representative data shown; $n=3$ independent experiments. **G**. The quantitative image of the apoptotic rate of nanoparticles^{TP53} on HCC cells. **H**. The quantitative image of the apoptotic rate of Anti-Her2 nanoparticles^{TP53} on Her2 + SK-OV-3 cells. **I**. The TP53 expression in Her2 + SK-OV-3 cells treated with different treatments. **J**. The Bcl-2 and Bax expression in Her2 + SK-OV-3 cells treated with different treatments

nanoparticles^{TP53} and nanoparticles^{TP53} are lower than those treated with blank nanoparticles and PBS, while the viability of anti-Her2 nanoparticles^{TP53} treatment is lower than nanoparticles^{TP53} treatment (Fig. 5C). Furthermore, as depicted in Fig. 5D in the apoptosis assay, the apoptotic rate of HCC$^{P53-/-}$ after the treatment with anti-Her2 EVs^{TP53} and nanoparticles^{TP53} are remarkable higher than that treated with blank nanoparticles and PBS. Meanwhile, there is no significant difference between the anti-Her2 nanoparticles^{TP53} treatment and nanoparticles^{TP53} treatment (Fig. 5E and G). Meanwhile, the apoptotic rate of Her2 + SKOV-3 cells treated with anti-Her2 nanoparticles^{TP53} and nanoparticles^{TP53} are higher than those treated with blank nanoparticles and PBS, while the viability of anti-Her2 nanoparticles^{TP53} treatment is higher than nanoparticles^{TP53} treatment (Fig. 5F and H). The western blot results showed anti-Her2 nanoparticles^{TP53} could deliver more TP53 proteins into the that the Her2 + SKOV-3 cells (Fig. 5I, Figure S2A and S2B), but could incite more apoptosis (Fig. 5I, Figure S2F, S2G and S2H). Collectively, the bioengineered anti-Her2 nanoparticles^{TP53} and nanoparticles^{TP53} could deliver the bioactive TP53 protein into both the artificial TP53-deficient cells and the native TP53-low cells and suppress the viability of these cancer cells in vitro, the specific nanoparticles could achieve the targeting delivery.

Anti-MSLN nanoparticles^{TP53} could inhibit TP53-low SKOV-3 xenograft models in vivo

To evaluate the therapeutic efficacy of specific targeting of nanoparticles^{TP53}, we performed in vivo study in immunocompromised athymic nude mice bearing native TP53-low SKOV-3 xenografts. Since MSLN is a glycoprotein anchored to the plasma membrane by a glycophosphatidyl inositol (GPI) domain. MSLN protein was found to be specifically expressed on ovarian cancer cells but not on normal human tissues, apart from mesothelial cells [55]. MSLN is emerging as an attractive target for cancer immunotherapy, considering its low expression on normal mesothelial cells and high expression in a broad spectrum of solid tumors. The MSLN-targeted immunotherapies reported to date support a favorable safety profile. MSLN is a potential CAR target in several common solid tumors [56]. We detected the targeting effect of anti-MSLN nanoparticles^{Cre} on MSLN + SKOV-3 cells by flowcytometry (Figure S3D) and TP53 delivery ability by western blot (Figure S2C, S2D and S2E). Then, we firstly used plasmid "Streptavidin-Lamp2b-PhoCl-TP53" to produce the SA-nanoparticles^{TP53}, and then incubated the SA-nanoparticles^{TP53} with biotin-anti-MSLN to produce the anti-MSLN nanoparticles^{TP53}. The tumor-burden nude mice were grouped into 4 groups: Control group (treated with PBS), Blank nanoparticles group, nanoparticles^{TP53} group and anti-MSLN nanoparticles^{TP53} group. The nanoparticles were systemically injected via tail vein every 3 days and for six times totally (Fig. 6A). As demonstrated in Fig. 6B, SKOV-3 tumor–bearing mice treated with PBS and blank nanoparticles showed rapid tumor growth, whereas nanoparticles^{TP53}treatment showed moderate antitumor activity. Encouragingly, anti-MSLN nanoparticles^{TP53} showed the highest anti-tumor effectiveness among these treatments (Fig. 6B and C). What's more, the tumor weights anti-MSLN nanoparticles^{TP53} treatment group are lower than those in nanoparticles^{TP53} treatment, blank EVs treatment and PBS treatment (Fig. 6D), while there is no significant difference of the body weights among these groups (Fig. 6E). According to the results from the immunofluorescence assay and the immunohistochemistry assay, the tumor from anti-MSLN nanoparticles^{TP53} expressed higher level of TP53 than other groups (Fig. 6F) and expressed lower level of Ki-67 than other groups (Fig. 6G). The anti-MSLN nanoparticles^{TP53} could also decrease the expression of IQGAP1, MYC and EGFR expression in ovarian cancer (Figure S4). These results indicate a potent anti-tumor effect of anti-MSLN nanoparticles^{TP53} in vivo. Above all, the specific targeting strategy of bioengineered nanoparticles could deliver the TP53 protein functionally into TP53-low SKOV-3 xenograft models in vivo with high efficiency.

Discussion

Increasing evidence have witnessed the critical role of *TP53* gene as a tumor suppressor gene involved in majority of cancers [57–59]. However, broad clinical translation will be enhanced by effective as well as specific targeting delivery platform in vivo [60]. Several approaches including LNP and AAV have been used to overcome the obstacle of delivering the TP53 protein for treating malignant cancers [6, 9]. Considering the repeating dosing which might increase the immune responses following by immune-related adverse reactions and treatment failure. Therefore, we selected the EVs-based nanoplatform as the delivery system. In this study, we developed an EVs-based nanoplatform with specific targeting ability to deliver TP53 proteins for ovarian cancer therapy. TP53 proteins could be effectively loaded into bioengineered EVs through plasmids transfection and biogenesis process. Then, we explored the SA-EVs incubated with antibodies showed vigorous specific targeting ability in ovarian cancer in vitro and ovarian cancer mouse models.

In the present study, we demonstrated that the nanoparticles could deliver diverse cargoes including GFP and luciferase proteins into receipt cells. This result is consistent with previous studies that Lamp2b could load cargoes into particles by plasmids transfection method [61, 62]. In addition, the nanoparticles could achieve the functional delivery including Cre recombinant protein to edit the Cre-Lxop sequence, which was widely used to detect the genome editing approaches [63–65]. These provide the theoretical evidence for TP53 biogenetic loading and functional delivery by bioengineered nanoplatforms. In addition, when we incubated the biotinylated-antibodies with the SA-nanoparticles, the specific targeting nanoparticles could enhance the delivering effectiveness in vitro and in vivo. The anti-Her2 nanoparticles^{Cre} could remarkably increase the delivery efficiency in Her2 + SKOV-3$^{Cre-Loxp}$ cells. Meanwhile, the anti-MSLN nanoparticles^{TP53} could exhibit greater anti-tumor effect in SKOV-3 cancer burden mice than nanoparticles^{TP53}. This result is consistent with previous studies that the expression of SA on the membrane of EVs exhibit a high affinity for biotinylated molecules for targeting delivery [66, 67].

IQGAP1 expresses high in most cancer and related to poor prognosis in ovarian cancer. In addition, IQGAP1 was correlated with immune-related genes and tumor-infiltrating lymphocytes. MYC-regulated pseudogene HMGA1P6 promotes ovarian cancer malignancy via augmenting the oncogenic HMGA1/2.The epithelial growth factor receptor (EGFR) family of receptor tyrosine kinases has been reported to have an active role in ovarian cancer [68]. And some studies reported the potential of drug delivery system targeting EGFR in ovarian cancer

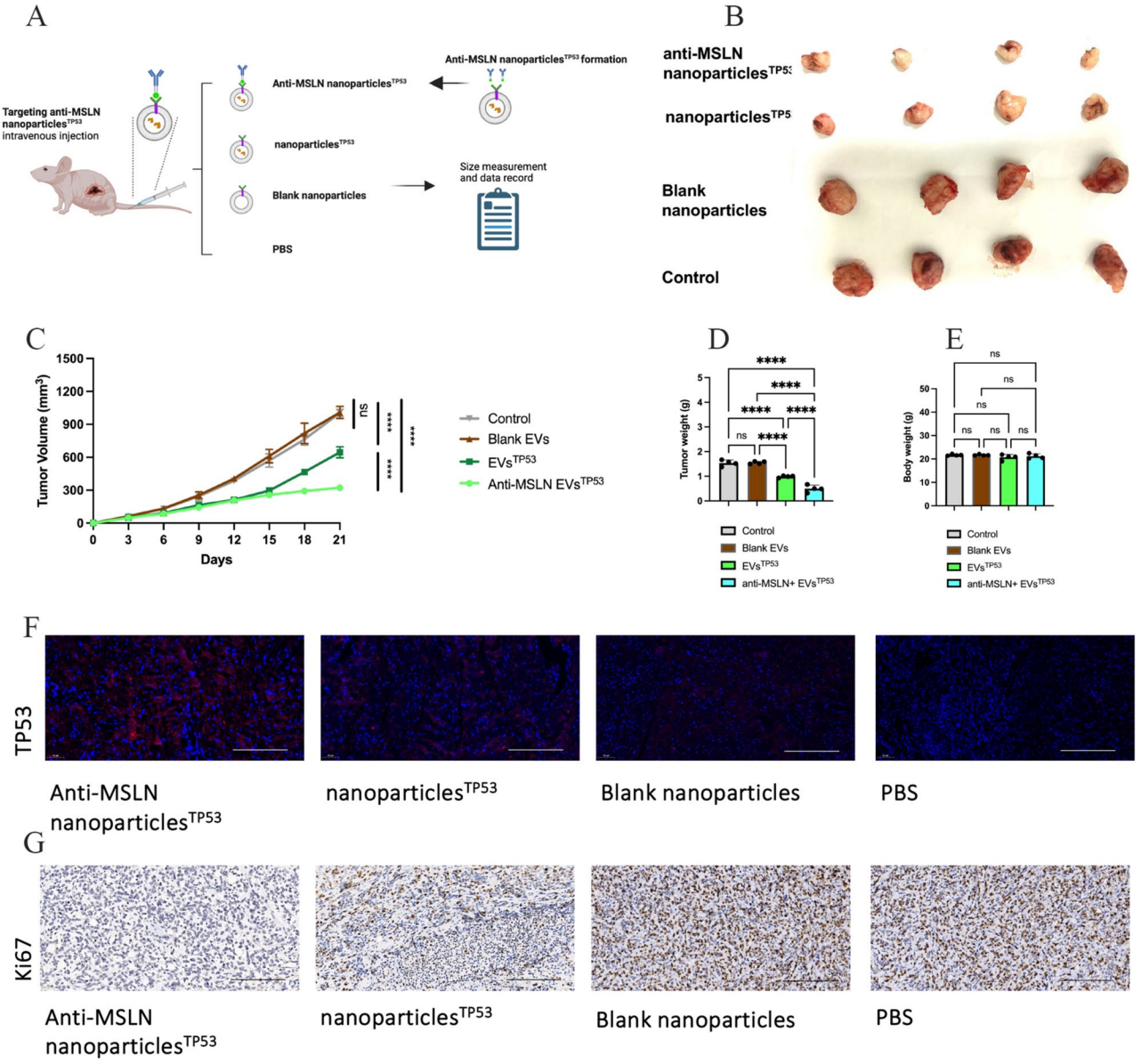

Fig. 6 Specific targeting anti-MSLN nanoparticles^{TP53} inhibit the ovarian cancer progression in vivo. **A**. Schematic image of the procedure to detect the effect of anti-MSLN nanoparticlesTP53 in ovarian cancer-bearing mouse model in vivo ($n=4$ per treatment group). **B**. The gross tumors resected from mice after diverse treatments. **C**. Tumor growth inhibition induced by anti-MSLN nanoparticles^{TP53}. **D**. Tumor weights inhibition induced by the anti-MSLN nanoparticles^{TP53}. **E**. The mice body weight after diverse treatments. **F**. The TP53 expression in tumor sections from mice after different treatments (Red: TP53, Blue: DAPI). Scale bar, 100 μm. **G**. The Ki67 expression in tumor sections from mice after different treatments. Scale bar, 100 μm

[69]. The result of this study is consistence with previous study that Synthetic mRNA nanoparticle-mediated restoration of p53 tumor suppressor sensitizes p53-deficient cancers to mTOR inhibition [6].

There are some limitations in this study. This study lacks related studies of different cargoes of nanoparticles (such as PTEN protein or cisplatin drugs), which might improve the efficiencies of cancer therapies. However, as the development the nanoparticles loading methods on modular surface design [70, 71] including click chemistry could improve the EVs-based nanoparticles mediated therapeutics.

Above all, our findings indicate that the bioengineered nanoparticles not only could load endogenous bioactive protein into the nanoparticles but also could release the cargoes into the recipient cells in a specific targeting way in vitro and in vivo. The TP53 protein could be delivered into TP53 deficient cancer cells and inhibit the viability of the cancer cell in vitro and in vivo. These results not only provide a practical strategy for TP53 delivery but

also open a promising avenue for the bioactive protein therapy of cancers.

Materials and methods

Cell lines

SKOV-3 and HCC$^{p53-/-}$ cells were purchased from Chinese Academy of Sciences. SKOV-3$^{Cre-LoxP}$ and Her2 + SKOV-3 were gifts from Shanghai Key Laboratory of Female Reproductive Endocrine Related Diseases. Cells were cultured in DMEM supplemented with 10% fetal bovine serum and 1% penicillin-streptomycin.

Plasmids design and synthesis

The "CD63-pEGFP C2" (addgene #62964) was used as a backbone for plasmids construction. The "pCAG-VSVG" (addgene #64084) was used for nanoparticles production. Codon-optimized DNA sequences for "Streptavidin", "Lamp2b", "Cre", "TP53" were ordered from IDT (Integrated DNA Technologies, USA) (sequences in Supplementary Table 1). The "PhoCl" was amplified from "pBAD/HisB-PhoCl-MBP" (addgene #87689). The "GFP" was amplified from "EGFP-mCherry" (addgene #193553). The "Luciferase" was amplified from "Luciferase" (addgene #213979). The constructs of "Lamp2b-PhoCl-Cre", "Lamp2b-PhoCl-TP53", "Lamp2b-PhoCl-Cre", "Lamp2b-PhoCl-Luciferase", "Lamp2b-PhoCl-GFP", "Streptavidin-Lamp2b" in this study were generated by the restriction enzyme digestion and subsequent self-ligation.

Plasmids transfection

HEK-293T cells were seeded overnight in T225 to reach 70% confluence. Plasmids were prepared for transfection. Plasmids at a weight ratio of 2:1 were pre-mixed with Hieff Trans® Liposomal Transfection Reagent (Yeasen Biotechnology (Shanghai) Co., Ltd) for transfection. The culture medium was changed as FBS-EVs-free DMEM medium after 4 h transfection.

Preparation of EVs and EVs^{TP53}

Firstly, FBS was centrifuged (100,000 g, 4℃ for 12 h) to remove EVs and isolate EVs-free FBS. Normally, HEK-293T cells were transfected with plasmids for 4 h and subsequently cultured in fresh DMEM (with 10% EVs-free FBS and 1% penicillin-streptomycin) for 48 h. EVs were isolated from the condition medium according to Thery's protocol [72]. Briefly, the condition medium was centrifuged at 300 g for 10 min, 10,000 g for 30 min, and 10,000 g for 75 min. All the collected pellet suspension were filtered by a 0.22-μm filter and then were transferred to new tubes with ultracentrifugation at 125 000 g for 120 min at 4 °C to pellet the extracellular vesicles by 70Ti rotor. All the produced engineered nanoparticles were treated with 405 nm violet light to cleave the PhoCl protein and release the free cargoes into the nanoparticles.

Characterization of nanoparticles and nanoparticles^{TP53}

The nanoparticles^{TP53} as well as blank nanoparticles were characterized by TEM, NTA and western blot, as previous reported [30, 73]. The morphology of isolated blank nanoparticles and nanoparticles^{TP53} were observed by transmission electron microscopy (FEI Tecnai G2 Spirit Twin, Philips, NL). The sizes of nanoparticles were measured by nanoparticle tracking analysis (NTA), using NanoSight NS300 (Malvern, Amesbury, GB). And the markers of nanoparticles including CD63, Alix, Tsg101 and GRP94 were detected by Western blot. The sorting protein Lamp2b and the cargo TP53 proteins were also detected by Western blot.

Uptake of the nanoparticles

SKOV-3 cells were seeded on autoclaved slides in a 24-well plate. Nanoparticles were stained with Cell Linker Kit for General Membrane Labeling reagent named PKH-26 (Sigma-Aldrich-PKH26GL) for 20 min and reisolated via ultracentrifugation. The PKH-26-labeled nanoparticles were added to the wells for 12 h. The cells were fixed with 4% paraformaldehyde for 20 min and stained with FITC-Actin Tracker (Beyotime, C2201S) for 0.5 h (following the manufacturer's instructions), followed by staining with DAPI for 10 min. Images were captured by confocal laser scanning microscopy (Leica Microsystems, Wetzlar, GER) at different laser channels. The images were analyzed and quantified via ImageJ software (NIH Image, Bethesda, MD).

Western blotting

Cell lysates and tumor tissues lysates were prepared to extracted proteins by using RIPA buffer. Proteins were separated by SDS–polyacylamide gel electrophoresis gel according to the standard procedure. The polyvinylidene difluoride membrane was incubated with 5% BSA for 1.5 h and then incubated with the antibody against TP53 (ab) and alpha-Tubulin (ab7291) at 4 °C overnight. After washing with 1 × TBST for three times, the membrane was incubated with HRP conjugated secondary antibodies. The membranes were visualized with enhanced chemiluminescence via an image capture (Amersham Imager 600). Nanoparticles (10^{10} per sample) were detected by CD63 (1:2000, ab134045), Alix (1:1000, ab275377), Tsg101 (1:2000, ab133586), GRP94 (1:1000, ab238126), Lamp2b (1 μg/mL, ab18529) and TP53 (1:4000, ab32389).

Biotinylation of SA-nanoparticles

Biotin–streptavidin (SA) binding offers a modular, high-affinity approach for protein bioconjugation [74]. Its versatility lies in the ability to biotinylate a wide variety of molecular and macromolecular systems, making it a robust platform for bioconjugation [75]. In our design, SA-Lamp2b fusion proteins were expressed on

nanoparticles, followed by the incubation of biotinylated antibodies with SA-overexpressing nanoparticles to generate targeted nanoparticles [76]. Anti-Her2 (ab134182) and anti-MSLN (ab309516) were purchased from Abcam. For biotinylation of anti-Her2, 500 μL of anti-Her2 (1 mg/mL) was mixed with 250 μL of biotin coupling solution and 250 μL of dissolved activated biotin. The mixture was allowed to react at room temperature for 1 h on a rotary suspension. The coupling mixture was transferred to the center of the desalinated resin column and centrifuged at 1000 ×g for 8 min. Biotin-anti-Her2 was collected in a centrifuge tube. For modification of SA-nanoparticles, biotin-anti-HER2 (2.5 μg/mL) and biotin-anti-MSLN (2.5 μg/mL) were incubated with SA-nanoparticles (100 μg protein/mL in PBS) at 37 ∘C for 30 min. The preparation of anti-MSLN nanoparticles is similar as above.

Luciferase detection assay

SKOV-3 cells were seeded in a six-well plate (10^6 cells/well) and treated with diverse nanoparticles for 24 h. To analyze luciferase activity, 10^6 cells were collected from the 6-well plate and suspended in 200 μL of Triton X-100 solution (0.2% in PBS). Subsequently, 50 μL of the sample was mixed with 50 μL of luciferase substrate (Promega, E1501) in a white-walled 96-well plate, following the manufacturer's instructions. The luciferase intensity in each well was then immediately measured through a Microplate Luminometer (GloMax, GM3000).

Flow cytometry assay

For cell apoptosis assay, 5×10^5 SKOV-3 cells and 5×10^5 $HCC^{p53-/-}$ cells were collected after $nanoparticles^{TP53}$ treatment for 48 h. Cell apoptosis was analyzed by flow cytometry using FITC-Annexin V and PI (BD Pharmingen, 556547) as recommended by the manufacturer. Data from at least 10^4 cells were acquired using CytoFLEX and the FlowJo software. For the delivery effect of nanoparticles, the $nanoparticles^{GFP}$ treated SKOV-3 cells were detected by flow cytometry to measure the percentage of GFP positive cells. Also, the $nanoparticles^{Cre}$ treated $SKOV\text{-}3^{Cre-Loxp}$ cells were detected by flow cytometry to measure the percentage of GFP positive cells.

Animals assay

In the animal assay, the nude mice were injected SKOV-3 cells (a total of 10^5 cells in 100 μL per mouse) subcutaneously to form bearing-tumor mice model. Three days later, diverse nanoparticles (10^{11} particles per mouse) were injected intravenously for every 3 days in totally 21 days. After 21 days injection, the tumor size, tumor weight and mice body weight were measured. The tumors were resected for subsequently immunofluorescence assay and IHC staining. Female nude mice (six weeks) were fed in the Laboratory in Animal house (the Obstetrics and Gynecology Hospital of Fudan University).

Immunofluorescence assay

The tumor tissues were embedded in paraffin and cut into 5μm sections. The slides were deparaffinized and rehydrated by xylene and different concentration of ethanol (100%, 95%, 80%, 70% and 50%). After the antigen repairment and blocking, anti-TP53 (1:100, ab32389) antibody and secondary antibody were added at room temperature. Slides were examined under a confocal immunofluorescence microscope (Zeiss).

Immunohistochemistry assay

Tissues were sectioned into 5 μm slices after being embedded in paraffin. Deparaffinization was performed using xylene, followed by rehydration through successive ethanol concentrations (100%, 95%, 80%, 70%, and 50%). After antigen retrieval and subsequent blocking, the slides were treated with the primary antibody against Ki67 (1 μg/mL, ab15580) at room temperature. The secondary antibody was applied subsequently. The stained sections were examined under a light microscope for visualization.

Data analysis

In this study, we conducted gene expression evaluation in cell line via Cancer Cell Line Encyclopedia (CCLE) DataSet (https://sites.broadinstitute.org/ccle/) and visualized the result by the depmap portal (https://depmap.org/portal/ccle/). Select tools of "Data Explorer" to analyze the TP53 expression in cell lines dataset.

Statistical analysis

All data were expressed as means ± standard deviation (SD). T-test was used for comparisons between two groups, and one-way analysis of variance (ANOVA) was applied for more than two groups. Statistical analysis was performed by Prism 9.2.0 software (GraphPad, San Diego, US). *, $P < 0.05$, **, $P < 0.01$, ***, $P < 0.001$, ****, $P < 0.0001$ was considered significant.

Supplementary Information

The online version contains supplementary material available at https://doi.org/10.1186/s13048-025-01672-9.

Supplementary Material 1: Supplementary Figure S1. The original membrane of western blot. The expression of markers and cargoes in diverse nanoparticles. The original gel and membrane of CD63, Tsg101, Alix, Lamp2b, GRP94 and TP53 in the engineered $nanoparticles^{TP53}$ and the blank nanoparticles.

Supplementary Material 2: Supplementary Figure S2. The original membrane of western blot. (A) The origin gel images of TP53 expression in Her2 + SK-OV-3 cells treated with different treatments. (B) The origin gel images of GAPDH expression in Her2 + SK-OV-3 cells treated with different treatments. (C) The TP53 expression in MSLN + SK-OV-3 cells treated

with different treatments. (D) The origin gel images of TP53 expression in MSLN + SK-OV-3 cells treated with different treatments. (E) The origin gel images of GAPDH expression in MSLN + SK-OV-3 cells treated with different treatments. (F) The origin gel images of Bcl-2 expression in Her2 + SK-OV-3 cells treated with different treatments. (G) The origin gel images of Bcl-2 expression in Her2 + SK-OV-3 cells treated with different treatments. (H) The origin gel images of GAPDH expression in Her2 + SK-OV-3 cells treated with different treatments.

Supplementary Material 3: Supplementary Figure S3. (A) The quantitative image of the editing efficiency of different number of nanoparticles^{Cre} in the SKOV-3$^{Cre-Loxp}$ cells in 96-well-plate. $p < 0.05$, $n = 3$. (B) The cell viability of SKOV-3 treated with the different number of nanoparticles^{Cre} i in 96-well-plate. $p < 0.05$, $n = 3$. (C) The Her2 expression in Her2 + SKOV-3 cells and HCC cells. (D) The quantitative image of the editing efficiency of anti-MSLN nanoparticles^{Cre} in the MSLN + SKOV-3$^{Cre-Loxp}$ cells. $p < 0.05$, $n = 3$.

Supplementary Material 4: Supplementary Figure S4. The IQGAP1, MYC and EGFR expression in tumor sections from mice after different nanoparticles treatments. Scale bar, 50 μm.

Supplementary Material 5

Author contributions

M.Z.: extract raw data, draft manuscript. Y.G. (Yuanyuan Gu): extract raw data, prepared Figs. 1, 2, 3, 4, 5 and 6, draft manuscript; F.S.: extract raw data. Y.G. (Yingxin Gong): extract raw data. G.Z.: edit manuscript. K.H.: read and edit manuscript. G.Z.: polish figures, review the main manuscript text. J.D.: review medical cord and data extraction, read, and edit manuscript. All authors reviewed the manuscript.

Funding

This study was supported by the Project of National Natural Science Foundation of China (No.81771524, No.81471416).

Data availability

No datasets were generated or analysed during the current study.

Declarations

Ethical approval

All animal procedures were performed in accordance with the protocol approved by the Institutional Animal Care and Use Committee at the Fudan University (SYXK2020-0032).

Competing interests

The authors declare no competing interests.

Author details

[1]Department of Gynecology, The Obstetrics and Gynecology Hospital of Fudan University, 419 Fang-Xie Road, Shanghai 200011, P.R. China
[2]Shanghai Key Laboratory of Female Reproductive Endocrine Related Diseases, Shanghai 200011, China

Received: 27 August 2024 / Accepted: 15 April 2025
Published online: 05 May 2025

References

1. Martins CP, Brown-Swigart L, Evan GI. Modeling the therapeutic efficacy of p53 restoration in tumors. Cell. 2006;127:1323–34.
2. Zhao D, Tahaney WM, Mazumdar A, Savage MI, Brown PH. Molecularly targeted therapies for p53-mutant cancers. Cell Mol Life Sci. 2017;74:4171–87.
3. Duffy MJ, Synnott NC, Crown J. Mutant p53 as a target for cancer treatment. Eur J Cancer. 2017;83:258–65.
4. Ghezelayagh TS, Kohrn BF, Fredrickson J, Krimmel-Morrison JD, Latorre-Esteves E, Tee XR, Radke MR, Manhardt E, Norquist BM, Katz R, et al. TP53 somatic evolution in cervical liquid-based cytology and blood from individuals with and without ovarian cancer and BRCA1 or BRCA2 germline mutations. Oncogene. 2024;43:2421–30.
5. Duchnowska R, Supernat AM, Pęksa R, Łukasiewicz M, Stokowy T, Ronen R, Dutkowski J, Umińska M, Iżycka-Świeszewska E, Kowalczyk A, et al. Pathway-level mutation analysis in primary high-grade serous ovarian cancer and matched brain metastases. Sci Rep. 2022;12:20537.
6. Kong N, Tao W, Ling X, Wang J, Xiao Y, Shi S, Ji X, Shajii A, Gan ST, Kim NY et al. Synthetic mRNA nanoparticle-mediated restoration of p53 tumor suppressor sensitizes p53-deficient cancers to mTOR Inhibition. Sci Transl Med. 2019;11.
7. Yoon AR, Lee S, Kim JH, Park Y, Koo T, Yun CO. CRISPR-mediated ablation of TP53 and EGFR mutations enhances gefitinib sensitivity and anti-tumor efficacy in lung cancer. Mol Ther 2024.
8. Muramatsu N, Ichikawa M, Katagiri T, Taguchi Y, Hatanaka T, Okuda T, Okamoto H. p53 dry gene powder enhances anti-cancer effects of chemotherapy against malignant pleural mesothelioma. Gene Ther. 2024;31:119–27.
9. Jiao Y, Tang Y, Li Y, Liu C, He J, Zhang LK, Guan YQ. Tumor cell-derived extracellular vesicles for breast cancer specific delivery of therapeutic P53. J Control Release. 2022;349:606–16.
10. Akeno N, Miller AL, Ma X, Wikenheiser-Brokamp KA. p53 suppresses carcinoma progression by inhibiting mTOR pathway activation. Oncogene. 2015;34:589–99.
11. Soragni A, Janzen DM, Johnson LM, Lindgren AG, Thai-Quynh Nguyen A, Tiourin E, Soriaga AB, Lu J, Jiang L, Faull KF, et al. A designed inhibitor of p53 aggregation rescues p53 tumor suppression in ovarian carcinomas. Cancer Cell. 2016;29:90–103.
12. Lei J, Cai M, Shen Y, Lin D, Deng X. Molecular dynamics study on the Inhibition mechanisms of ReACp53 peptide for p53-R175H mutant aggregation. Phys Chem Chem Phys. 2021;23:23032–41.
13. Zhang Y, Hu Y, Wang JL, Yao H, Wang H, Liang L, Li C, Shi H, Chen Y, Fang JY, Xu J. Proteomic identification of ERP29 as a key chemoresistant factor activated by the aggregating p53 mutant Arg282Trp. Oncogene. 2017;36:5473–83.
14. Neal A, Lai T, Singh T, Rahseparian N, Grogan T, Elashoff D, Scott P, Pellegrini M, Memarzadeh S. Combining ReACp53 with carboplatin to target High-Grade serous ovarian cancers. Cancers (Basel) 2021;13.
15. Zong Y, Lin Y, Wei T, Cheng Q. Lipid nanoparticle (LNP) enables mRNA delivery for Cancer therapy. Adv Mater. 2023;35:e2303261.
16. Wang D, Tai PWL, Gao G. Adeno-associated virus vector as a platform for gene therapy delivery. Nat Rev Drug Discov. 2019;18:358–78.
17. Khan MM, Filipczak N, Torchilin VP. Cell penetrating peptides: A versatile vector for co-delivery of drug and genes in cancer. J Control Release. 2021;330:1220–8.
18. Herrmann IK, Wood MJA, Fuhrmann G. Extracellular vesicles as a next-generation drug delivery platform. Nat Nanotechnol. 2021;16:748–59.
19. Ma X, Liang X, Li Y, Feng Q, Cheng K, Ma N, Zhu F, Guo X, Yue Y, Liu G, et al. Modular-designed engineered bacteria for precision tumor immunotherapy via Spatiotemporal manipulation by magnetic field. Nat Commun. 2023;14:1606.
20. Maugeri M, Nawaz M, Papadimitriou A, Angerfors A, Camponeschi A, Na M, Hölttä M, Skantze P, Johansson S, Sundqvist M, et al. Linkage between endosomal escape of LNP-mRNA and loading into EVs for transport to other cells. Nat Commun. 2019;10:4333.
21. Xu X, Chen W, Zhu W, Chen J, Ma B, Ding J, Wang Z, Li Y, Wang Y, Zhang X. Adeno-associated virus (AAV)-based gene therapy for glioblastoma. Cancer Cell Int. 2021;21:76.
22. Asrorov AM, Wang H, Zhang M, Wang Y, He Y, Sharipov M, Yili A, Huang Y. Cell penetrating peptides: highlighting points in cancer therapy. Drug Dev Res. 2023;84:1037–71.
23. Théry C, Witwer KW, Aikawa E, Alcaraz MJ, Anderson JD, Andriantsitohaina R, Antoniou A, Arab T, Archer F, Atkin-Smith GK, et al. Minimal information for studies of extracellular vesicles 2018 (MISEV2018): a position statement of the international society for extracellular vesicles and update of the MISEV2014 guidelines. J Extracell Vesicles. 2018;7:1535750.
24. Zhang R, Fu Y, Cheng M, Ma W, Zheng N, Wang Y, Wu Z. sEVs(RVG) selectively delivers antiviral SiRNA to fetus brain, inhibits ZIKV infection and mitigates ZIKV-induced microcephaly in mouse model. Mol Ther. 2022;30:2078–91.
25. Zhang H, Freitas D, Kim HS, Fabijanic K, Li Z, Chen H, Mark MT, Molina H, Martin AB, Bojmar L, et al. Identification of distinct nanoparticles and subsets of extracellular vesicles by asymmetric flow field-flow fractionation. Nat Cell Biol. 2018;20:332–43.
26. Kenific CM, Zhang H, Lyden D. An exosome pathway without an ESCRT. Cell Res. 2021;31:105–6.
27. Yang Z, Ji P, Li Z, Zhang R, Wei M, Yang Y, Yuan L, Han Y, Yang G. Improved extracellular vesicle-based mRNA delivery for Familial hypercholesterolemia treatment. Theranostics. 2023;13:3467–79.

28. Hung ME, Leonard JN. A platform for actively loading cargo RNA to elucidate limiting steps in EV-mediated delivery. J Extracell Vesicles. 2016;5:31027.
29. Zhou G, Gu Y, Zhou F, Zhang H, Zhang M, Zhang G, Wu L, Hua K, Ding J. Adipocytes-Derived extracellular Vesicle-miR-26b promotes apoptosis of cumulus cells and induces polycystic ovary syndrome. Front Endocrinol (Lausanne). 2021;12:789939.
30. Zhu Z, Zhang Y, Zhang Y, Zhang H, Liu W, Zhang N, Zhang X, Zhou G, Wu L, Hua K, Ding J. Exosomes derived from human umbilical cord mesenchymal stem cells accelerate growth of VK2 vaginal epithelial cells through MicroRNAs in vitro. Hum Reprod. 2019;34:248–60.
31. Zheng W, Rädler J, Sork H, Niu Z, Roudi S, Bost JP, Görgens A, Zhao Y, Mamand DR, Liang X, et al. Identification of scaffold proteins for improved endogenous engineering of extracellular vesicles. Nat Commun. 2023;14:4734.
32. Elsharkasy OM, Nordin JZ, Hagey DW, de Jong OG, Schiffelers RM, Andaloussi SE, Vader P. Extracellular vesicles as drug delivery systems: why and how? Adv Drug Deliv Rev. 2020;159:332–43.
33. Peinado H, Zhang H, Matei IR, Costa-Silva B, Hoshino A, Rodrigues G, Psaila B, Kaplan RN, Bromberg JF, Kang Y, et al. Pre-metastatic niches: organ-specific homes for metastases. Nat Rev Cancer. 2017;17:302–17.
34. Liu C, Lu J, Tian H, Du W, Zhao L, Feng J, Yuan D, Li Z. Increased expression of PD–L1 by the human papillomavirus 16 E7 oncoprotein inhibits anticancer immunity. Mol Med Rep. 2017;15:1063–70.
35. Kalluri R. The biology and function of extracellular vesicles in immune response and immunity. Immunity. 2024;57:1752–68.
36. Hoshino A, Costa-Silva B, Shen TL, Rodrigues G, Hashimoto A, Tesic Mark M, Molina H, Kohsaka S, Di Giannatale A, Ceder S, et al. Tumour exosome integrins determine organotropic metastasis. Nature. 2015;527:329–35.
37. Osteikoetxea X, Silva A, Lázaro-Ibáñez E, Salmond N, Shatnyeva O, Stein J, Schick J, Wren S, Lindgren J, Firth M, et al. Engineered Cas9 extracellular vesicles as a novel gene editing tool. J Extracell Vesicles. 2022;11:e12225.
38. Costa Verdera H, Gitz-Francois JJ, Schiffelers RM, Vader P. Cellular uptake of extracellular vesicles is mediated by clathrin-independent endocytosis and macropinocytosis. J Control Release. 2017;28:100–8.
39. Bevers S, Kooijmans SAA, Van de Velde E, Evers MJW, Seghers S, Gitz-Francois J, van Kronenburg NCH, Fens M, Mastrobattista E, Hassler L, et al. mRNA-LNP vaccines tuned for systemic immunization induce strong antitumor immunity by engaging Splenic immune cells. Mol Ther. 2022;30:3078–94.
40. Kooijmans SAA, Stremersch S, Braeckmans K, de Smedt SC, Hendrix A, Wood MJA, Schiffelers RM, Raemdonck K, Vader P. Electroporation-induced SiRNA precipitation obscures the efficiency of SiRNA loading into extracellular vesicles. J Control Release. 2013;172:229–38.
41. Wahlgren J, Statello L, Skogberg G, Telemo E, Valadi H. Delivery of small interfering RNAs to cells via exosomes. Methods Mol Biol. 2016;1364:105–25.
42. Wahlgren J, De LKT, Brisslert M, Vaziri Sani F, Telemo E, Sunnerhagen P, Valadi H. Plasma exosomes can deliver exogenous short interfering RNA to monocytes and lymphocytes. Nucleic Acids Res. 2012;40:e130.
43. Larios J, Mercier V, Roux A, Gruenberg J. ALIX- and ESCRT-III–dependent sorting of tetraspanins to exosomes. J Cell Biol. 2022;219:e201904113.
44. Salunkhe S, Dheeraj, Basak M, Chitkara D, Mittal A. Surface functionalization of exosomes for target-specific delivery and in vivo imaging & tracking: strategies and significance. J Control Release. 2020;326:599–614.
45. Han J, Sul JH, Lee J, Kim E, Kim HK, Chae M, Lim J, Kim J, Kim C, Kim JS, et al. Engineered exosomes with a photoinducible protein delivery system enable CRISPR-Cas-based epigenome editing in Alzheimer's disease. Sci Transl Med. 2024;16:eadi4830.
46. Pei W, Zhang Y, Zhu X, Zhao C, Li X, Lü H, Lv K. Multitargeted Immunomodulatory therapy for viral myocarditis by engineered extracellular vesicles. ACS Nano. 2024;18:2782–99.
47. Joshi BS, de Beer MA, Giepmans BNG, Zuhorn IS. Endocytosis of extracellular vesicles and release of their cargo from endosomes. ACS Nano. 2020;14:4444–55.
48. Fan Y, Pionneau C, Cocozza F, Boëlle PY, Chardonnet S, Charrin S, Théry C, Zimmermann P, Rubinstein E. Differential proteomics argues against a general role for CD9, CD81 or CD63 in the sorting of proteins into extracellular vesicles. J Extracell Vesicles. 2023;12:e12352.
49. Kashyap P, Bertelli S, Cao F, Kostritskaia Y, Blank F, Srikanth NA, Schlack-Leigers C, Saleppico R, Bierhuizen D, Lu X, et al. An optogenetic method for the controlled release of single molecules. Nat Methods. 2024;21:666–72.
50. Ghandi M, Huang FW, Jané-Valbuena J, Kryukov GV, Lo CC, McDonald ER 3rd, Barretina J, Gelfand ET, Bielski CM, Li H, et al. Next-generation characterization of the Cancer cell line encyclopedia. Nature. 2019;569:503–8.
51. Pharmacogenomic agreement between. Two cancer cell line data sets. Nature. 2015;528:84–7.
52. Xiao Y, Chen J, Zhou H, Zeng X, Ruan Z, Pu Z, Jiang X, Matsui A, Zhu L, Amoozgar Z, et al. Combining p53 mRNA nanotherapy with immune checkpoint Blockade reprograms the immune microenvironment for effective cancer therapy. Nat Commun. 2022;13:758.
53. Zeimet AG, Marth C. Why did p53 gene therapy fail in ovarian cancer? Lancet Oncol. 2003;4:415–22.
54. Sjöqvist S, Ishikawa T, Shimura D, Kasai Y, Imafuku A, Bou-Ghannam S, Iwata T, Kanai N. Exosomes derived from clinical-grade oral mucosal epithelial cell sheets promote wound healing. J Extracell Vesicles. 2019;8:1565264.
55. Chang K, Pai LH, Batra JK, Pastan I, Willingham MC. Characterization of the antigen (CAK1) recognized by monoclonal antibody K1 present on ovarian cancers and normal mesothelium. Cancer Res. 1992;52:181–6.
56. Morello A, Sadelain M, Adusumilli PS. Mesothelin-Targeted cars: driving T cells to solid tumors. Cancer Discov. 2016;6:133–46.
57. Izquierdo E, Vorholt D, Blakemore S, Sackey B, Nolte JL, Barbarino V, Schmitz J, Nickel N, Bachurski D, Lobastova L, et al. Extracellular vesicles and PD-L1 suppress macrophages, inducing therapy resistance in TP53-deficient B-cell malignancies. Blood. 2022;139:3617–29.
58. Ma Q, Liu Y, Zhao H, Guo Y, Sun W, Hu R. Variation characteristics and clinical significance of TP53 in patients with myeloid neoplasms. Hematology. 2024;29:2387878.
59. Tee XR, Hazard E, Latorre-Esteves E, Kohrn BF, Ghezelayagh TS, Fredrickson JU, Coombes C, Radke MR, Manhardt E, Katz R, et al. Increased TP53 somatic evolution in peritoneal washes of individuals with BRCA1 germline mutations. Gynecol Oncol. 2024;190:18–27.
60. Tasdemir E, Maiuri MC, Galluzzi L, Vitale I, Djavaheri-Mergny M, D'Amelio M, Criollo A, Morselli E, Zhu C, Harper F, et al. Regulation of autophagy by cytoplasmic p53. Nat Cell Biol. 2008;10:676–87.
61. Wang C, Li N, Li Y, Hou S, Zhang W, Meng Z, Wang S, Jia Q, Tan J, Wang R, Zhang R. Engineering a HEK-293T exosome-based delivery platform for efficient tumor-targeting chemotherapy/internal irradiation combination therapy. J Nanobiotechnol. 2022;20:247.
62. Bi W, Mu X, Li Y, Sun Q, Xiang L, Hu M, Liu H. Delivery of neurotrophin-3 by RVG-Lamp2b-modified mesenchymal stem cell-derived exosomes alleviates facial nerve injury. Hum Cell. 2024;37:1378–93.
63. Zomer A, Maynard C, Verweij FJ, Kamermans A, Schäfer R, Beerling E, Schiffelers RM, de Wit E, Berenguer J, Ellenbroek SIJ, et al. In vivo imaging reveals extracellular vesicle-mediated phenocopying of metastatic behavior. Cell. 2015;161:1046–57.
64. Bittel M, Reichert P, Sarfati I, Dressel A, Leikam S, Uderhardt S, Stolzer I, Phu TA, Ng M, Vu NK, et al. Visualizing transfer of microbial biomolecules by outer membrane vesicles in microbe-host-communication in vivo. J Extracell Vesicles. 2021;10:e12159.
65. Zomer A, Steenbeek SC, Maynard C, van Rheenen J. Studying extracellular vesicle transfer by a Cre-loxP method. Nat Protoc. 2016;11:87–101.
66. Meng W, Wang L, Du X, Xie M, Yang F, Li F, Wu ZE, Gan J, Wei H, Cao C, et al. Engineered mesenchymal stem cell-derived extracellular vesicles constitute a versatile platform for targeted drug delivery. J Control Release. 2023;363:235–52.
67. Jayasinghe MK, Pirisinu M, Yang Y, Peng B, Pham TT, Lee CY, Tan M, Vu LT, Dang XT, Pham TC, et al. Surface-engineered extracellular vesicles for targeted delivery of therapeutic RNAs and peptides for cancer therapy. Theranostics. 2022;12:3288–315.
68. Sheng Q, Liu J. The therapeutic potential of targeting the EGFR family in epithelial ovarian cancer. Br J Cancer. 2011;104:1241–5.
69. Xi X, Lei F, Gao K, Li J, Liu R, Karpf AR, Bronich TK. Ligand-installed polymeric nanocarriers for combination chemotherapy of EGFR-positive ovarian cancer. J Control Release. 2023;360:872–87.
70. Strebinger D, Frangieh CJ, Friedrich MJ, Faure G, Macrae RK, Zhang F. Cell type-specific delivery by modular envelope design. Nat Commun. 2023;14:5141.
71. Stranford DM, Simons LM, Berman KE, Cheng L, DiBiase BN, Hung ME, Lucks JB, Hultquist JF, Leonard JN. Genetically encoding multiple functionalities into extracellular vesicles for the targeted delivery of biologics to T cells. Nat Biomed Eng 2023.
72. Théry CA-O, Witwer KA-O, Aikawa E, Alcaraz MJ, Anderson JD, Andriantsitohaina R, Antoniou A, Arab T, Archer F, Atkin-Smith GK, et al. Minimal information for studies of extracellular vesicles 2018 (MISEV2018): a position statement of the international society for extracellular vesicles and update of the MISEV2014 guidelines. J Extracell Vesicles. 2018;7:1535750.

73. Zhou G, Gu Y, Zhu Z, Zhang H, Liu W, Xu B, Zhou F, Zhang M, Hua K, Wu L, Ding J. Exosome mediated cytosolic cisplatin delivery through Clathrin-Independent endocytosis and enhanced Anti-cancer effect via avoiding endosome trapping in cisplatin-Resistant ovarian Cancer. Front Med (Lausanne). 2022;9:810761.
74. Schendel LC, Sedlak SM, Gaub HE. Switchable reinforced Streptavidin. Nanoscale. 2020;12:6803–9.
75. Reznik GO, Vajda S, Cantor CR, Sano T. A Streptavidin mutant useful for directed immobilization on solid surfaces. Bioconjug Chem. 2001;12:1000–4.
76. Luther DC, Lee YW, Nagaraj H, Clark V, Jeon T, Goswami R, Gopalakrishnan S, Fedeli S, Jerome W, Elia JL, Rotello VM. Cytosolic protein delivery using modular Biotin-Streptavidin assembly of nanocomposites. ACS Nano. 2022;16:7323–30.

Publisher's note